

HI absorption in a gravitational lens at $z \sim 0.7645$

N. Kanekar¹* F. H. Briggs²**

¹ Kapteyn Institute, University of Groningen, Postbus 800, 9700 AV Groningen, The Netherlands

² RSAA, The Australian National University, Mount Stromlo Observatory, Cotter Road, ACT 2611, Australia

Received mmddyy/ accepted mmddyy

Abstract. We have used the Westerbork Synthesis Radio Telescope to detect HI 21cm absorption at $z \sim 0.7645$ in the gravitational lens system towards PMN J0134–0931. The 21cm profile has two broad components, with peak optical depths of 0.047 ± 0.007 and 0.039 ± 0.007 , at heliocentric redshifts 0.76470 ± 0.00006 and 0.76348 ± 0.00006 , respectively. The redshift of the stronger component matches that of CaII H and K absorption detected earlier. The absorption has a total velocity width of $\sim 500 \text{ km s}^{-1}$ (between nulls) and an equivalent width of $7.1 \pm 0.08 \text{ km s}^{-1}$. This would imply a total HI column density of $2.6 \pm 0.3 \times 10^{21} \text{ cm}^{-2}$, for a spin temperature of 200 K and a covering factor of unity. The high estimated HI column density is consistent with the presence of large amounts of dust at the lens redshift; the intervening dust could be responsible for the extremely red colour of the background quasar.

Key words. Galaxies: individual: PMN J0134–0931 – gravitational lensing – radio lines – ISM

1. Introduction

The $z \sim 2.2$ radio-loud quasar PMN J0134–0931 is an exceedingly interesting object. Its radio continuum consists of at least 6 components, with a maximum image separation of $\sim 700 \text{ mas}$ (Winn et al. 2002 (W02); Winn et al. 2003 (W03)). Five of these images (A – E) have the same spectral index and a curved arc of emission is seen between A and B. These properties caused W02 to argue that the object is a gravitationally lensed system. Similarly, Gregg et al. (2002) used the multiplicity of components in a near-IR image as well as the high inferred source luminosity as evidence for lensing. Interestingly enough, PMN J0134–0931 is only the second lens of galactic mass to show an image multiplicity greater than four; the other such lens is the six-component system towards CLASS B1359+154 (Rusin et al. 2001).

CaII H and K lines have been detected towards PMN J0134–0931, at $z = 0.76451 \pm 0.00016$ (Hall et al. 2002); the lens is thus likely to be at this redshift. The CaII absorption is very strong, with rest frame equivalent width $\sim 5.3 \text{ \AA}$, similar to that seen in the lens B0218+357 (Browne et al. 1993). Further, the quasar is highly reddened in optical wavebands, with $B - K \geq 11$ (Gregg et al. 2002); this suggests the presence of large amounts of dust, either in the host galaxy of the quasar or in the lensing galaxy. While the differential extinction of the quasar images suggests that at least some of the reddening is due to dust in the absorber, it has so far not been possible to conclusively determine the location of the dust. Assuming the

dust is at $z = 0.7645$ implies $E(B - V) = 1.315$, i.e. a visual extinction $A_V = 3.85$ (Hall et al. 2002). In conjunction with the strong CaII lines, this would suggest that the lens is a gas-rich, late-type galaxy.

More recently, Keeton & Winn (2003) have come up with the first quantitative model of the lensing system that explains most of its observed properties. The background source is assumed to have two components and the lensing system to consist of two galaxies. The observed 5 components A – E are then the images of one of the background sources and component F is an image of the second, with the remaining two images of the latter source too faint for detection. The model is supported by new high-resolution radio and optical observations (W03), which found that F has a different spectral index from images A – E. These observations also showed that the observed large sizes of components C and E are not intrinsic but instead arise due to scatter broadening at the lower frequencies. Finally, W03 find marginal evidence for a detection of the two lens galaxies in Hubble Space Telescope (HST) images of the system; Keeton & Winn (2003) predict these to be spiral galaxies, each with a velocity dispersion of about $\sim 120 \text{ km s}^{-1}$, and a projected separation of $\sim 0.4''$.

We present, in this Letter, Westerbork Synthesis Radio Telescope (WSRT) observations of HI 21cm absorption at $z \sim 0.7645$ towards PMN J0134–0931. The usual association of dust with high column densities of neutral gas confirms that the dust is likely to be concentrated in the intervening lens system. We describe the WSRT observations and data analysis in section 2; the spectra, results and models are presented and discussed in section 3.

Send offprint requests to: Nissim Kanekar

* nissim@astro.rug.nl

** fbriggs@mso.anu.edu.au

2. Observations and data analysis

PMN J0134–0931 was observed with the UHF-High band of the WSRT on March 28 and 31 and July 5 and 7, 2003, with the DZB correlator as the backend. A single 5 MHz IF band was used on all occasions, sub-divided into 1024 channels and centred at an observing frequency of 805 MHz; this yielded a frequency resolution of ~ 4.88 kHz, i.e. a velocity resolution of ~ 1.8 km s $^{-1}$. The standard calibrators 3C48 and 3C147 were used to calibrate the absolute flux density scale at all observing epochs; their adopted flux densities are on the scale of Baars et al. (1977). The system bandpass was calibrated with observations of 3C48, 3C147, 3C454.3 or 3C138. All fourteen WSRT antennas were available for the observations in all observing runs. The total on-source time was 17.6 hours.

The data were converted from the telescope format to FITS and then analyzed in classic AIPS, using standard techniques. Data from the March and July runs were analyzed separately and self-calibrated independently. Spectra from the two epochs were corrected to the heliocentric frame outside AIPS and then averaged together. The flux density of PMN J0134–0931 was measured to be 590 ± 2 mJy on all observing runs.

We note that two strong, narrow RFI spikes were found to be present not far from the expected location of the redshifted 21cm line; these were seen in both the March and July runs, at the same observing frequencies (i.e. shifted heliocentric frequencies). The high initial spectral resolution of the observations limited the effect of these spikes on neighbouring channels; the data were also Hanning smoothed in frequency, to further reduce spectral ringing.

3. Discussion

3.1. The 21cm spectrum and derived quantities

The final WSRT HI 21cm spectrum towards PMN J0134–0931 is shown in figure 1; this has been boxcar smoothed by three channels (and re-sampled) and has a velocity resolution of ~ 10.8 km s $^{-1}$ and an RMS noise of ~ 4.1 mJy. The redshift of the CaII lines (Hall et al. 2002) is shown below the spectrum, with error bars.

Two deep features can be immediately identified in the spectrum of Fig. 1, with their peak optical depths at heliocentric frequencies of 804.898 ± 0.03 and 805.455 ± 0.03 MHz, i.e. heliocentric redshifts of 0.76470 ± 0.00006 and 0.76348 ± 0.00006 respectively. The redshift of the first of these features agrees with that of the CaII lines, within the errors. This is also the deeper of the two HI components, with a peak optical depth of 0.047 ± 0.007 ; the second feature has a peak optical depth of 0.039 ± 0.007 . The HI absorption is extremely wide, with a total velocity spread (between nulls) of ~ 500 km s $^{-1}$. This is similar to the width of the CaII lines, which have $\sigma_v = 220 \pm 40$ km s $^{-1}$ (Hall et al. 2002).

The equivalent width of the 21cm profile is $\int \tau_{21} dV = 7.06 \pm 0.08$ km s $^{-1}$. This is higher than that measured in either of the other gravitational lenses in which HI absorption has so far been detected, B0218+357 ($EW = 2.94 \pm 0.02$ km s $^{-1}$; Kanekar et al. 2003) and PKS 1830–21 ($EW =$

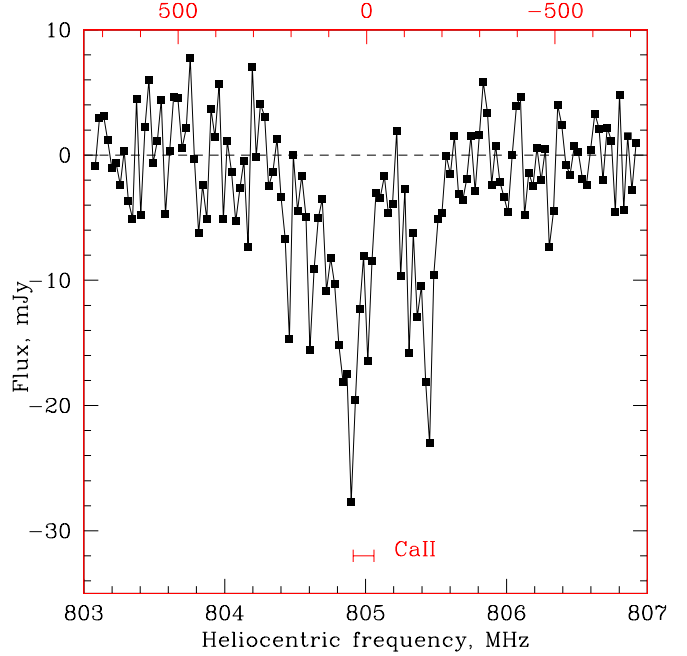


Fig. 1. Final WSRT HI 21cm spectrum towards PMN J0134–0931. The x and y axes are heliocentric frequency (in MHz) and flux density (in mJy) respectively; the top axis is heliocentric velocity (in km s $^{-1}$), relative to $z = 0.7645$. The spectrum has been boxcar smoothed by 3 channels and has a velocity resolution of ~ 10.8 km s $^{-1}$ and an RMS noise of ~ 4.1 mJy.

5.8 ± 0.4 km s $^{-1}$; Chengalur et al. 1999). The large equivalent width implies a very HI column density $N_{\text{HI}} = 2.6 \pm 0.3 \times 10^{21} (T_s/200\text{K})(1/f)$ cm $^{-2}$ (e.g. Kanekar & Chengalur 2003), where f is the covering factor of the absorber and T_s , its spin temperature; this is well into the range observed in damped Lyman- α systems (e.g. Wolfe et al. 1986). We note that a spin temperature of ~ 200 K is typical of spiral galaxies, both locally (Braun & Walterbos 1992) and at low redshift (Kanekar & Chengalur 2003). Of course, the above estimate of N_{HI} gives the sum of HI column densities towards *all* the different source components giving rise to the 21cm absorption; it is not possible to measure the column density towards individual source components with the available data.

The extremely high estimated HI column density implies a high dust content in the $z \sim 0.7645$ lens and explains the observed reddening in the optical images (Gregg et al. 2002; W03). Assuming that the molecular hydrogen column density is roughly equal to N_{HI} , the total hydrogen column density $N_{\text{H}} = 2N_{\text{H}_2} + N_{\text{HI}} \sim 7.8 \times 10^{21}$ cm $^{-2}$ (again assuming $T_s = 200$ K and a covering factor of unity). This implies $E(B - V) \sim 1.35$, using a Galactic dust to gas ratio; further assuming a Galactic extinction law ($R_V = 3.1$; Binney & Merrifield 1998) results in a visual extinction $A_V \sim 4.15$. Of course, it is likely that the 21cm absorption profile (and hence the estimated column density) contains contributions from more than one line of sight, with variable optical depth and kinematics across the

complex lensing image; it is thus not possible to estimate the visual extinction towards individual source components.

3.2. Modelling the absorption

The lens towards PMN J0134–0931 creates a complex radio image of six image components (A – F), with a maximum angular separation of ~ 681 mas (W02). Components A and B are seen to connect in a section of lensing arc at faint levels in the 1.7 GHz VLBA image (W03). Components C and E appear to be strongly scatter broadened at frequencies below 5 GHz and are almost undetected in VLBA images at 1.7 GHz (W02,W03), as they are over-resolved by even the shortest baselines of the VLBA. Note, however, that their flux must be present in the integral flux density measured in our spectrum at 805 MHz; further, they provide additional lines of sight through the $z \sim 0.7645$ absorber. Next, while component F has a significantly steeper spectrum than the other five components, its total flux density is only 11 ± 1 mJy at 1.7 GHz; it is thus quite unlikely to have sufficient flux density at 805 MHz to give rise to either of the two main 21cm components. Further, while it is possible that the some of the wide, weak absorption arises against this component, this would require a fairly high optical depth ($\tau \gtrsim 0.5$). The 21cm absorption is thus most likely to arise against the brighter components A, B, C and D (and perhaps the arc of radio emission between A and B), each of which have flux densities $\gtrsim 100$ mJy at 1.7 GHz. We note that component A also shows evidence for scatter broadening at frequencies below 5 GHz while D is the most strongly reddened of the source components; on the other hand, B is the bluest of all components and shows no evidence for scatter broadening in the VLBA images (W03). This suggests that there is relatively less dust and gas along the line of sight to component B; the two main 21cm features thus appear most likely to arise from absorption against components A and D.

We have explored these possibilities with a simple kinematic model using a differentially rotating disk absorber. The modelling does not produce a unique result, but rather succeeds in demonstrating that a single, massive galaxy could indeed be responsible for the 21cm absorption profile. If a more complex, multi-galaxy system were to be invoked, there would be ample free parameters to fit the integral spectrum reported here. Further observational progress will require radio interferometry to separate the absorption along different lines of sight.

The philosophy of modelling the 21cm profile shape is based on the assumption that narrow absorption features occur in the spectrum when a compact, high-surface brightness image of the background radio source “selects” a small patch from an extended, smooth velocity field of a rotating galaxy. Thus, the two main narrow 21cm features of Fig. 1 are expected to be associated with specific source components of the background source, once VLBI observations are conducted in the 21 cm line. The modelling uses the source structure obtained from the 1.7 GHz VLBA maps of W03 for the compact radio components, with a scaling in flux to both match the relative flux densities of the components in the higher frequency bands, and still produce the integral flux density measured at 805 MHz by our

WSRT observations. The more extended components C and E had to be supplemented with diffuse gaussian components to account for the flux missing from the VLBA map.

The two models discussed here (and shown in Fig. 2[B]) are representative of two broad classes which can reproduce the observed 21cm profile. It should be emphasized, however, that neither class is able to account for *all* the observations simultaneously, including the scatter broadening and reddening of different source components. Both models are axially symmetric, planar systems with rotation curves that are flat at V_{rot} in the outer regions, with a linear rise from the centre to R_c . The systemic velocity of the galaxy is offset from 805 MHz ($z = 0.76448$) by V_{off} , and the galaxy centroid is specified by the projected positional offsets ΔX (west), ΔY (north) relative to image D. The HI optical depth profile for each pixel is broadened by a velocity dispersion of $\sigma_v = 7$ km s $^{-1}$ before computing that pixel’s contribution to the integral absorption spectrum.

3.2.1. Model I

Models belonging to class I are motivated by the need to inflict heavy reddening on image D without reddening B, coupled with accounting for the scatter broadening of A and C. However, this model does not account for the scatter broadening of image E. The model parameters are: position angle of the receding major axis $p = -50^\circ$ ($+p$, measured east from north), inclination to sky plane $i = 85^\circ$, $V_{\text{rot}} = 230$ km s $^{-1}$, $R_c = 1.4$ kpc, exponential gas scale height $h = 0.7$ kpc, $V_{\text{off}} = 35$ km s $^{-1}$, and galaxy position at $\Delta X = 490$ mas, $\Delta Y = 370$ mas. In this highly inclined model, the HI column density measured perpendicular to the galaxy plane is only $3 \times 10^{19} (T_s/100)$ cm $^{-2}$ in the region that covers components A and C, but it rises to $3 \times 10^{20} (T_s/100)$ cm $^{-2}$ for B and D. The high disk inclination increases the line of sight column densities by an order of magnitude. The 21cm spectrum resulting from this model is shown in fig. 2[A]. Here, the two narrow features arise from absorption against A and D; the extended weak absorption wing out to $\sim +300$ km s $^{-1}$ is achieved by tipping the intervening disk to a high inclination and thickening the HI layer with a scale height of ~ 700 pc (in the spirit of Briggs et al. (1985) and Prochaska and Wolfe (1997)).

3.2.2. Model II

The second, somewhat orthogonal, class of models (of which Model II is an example) has an infinitesimally thin disk, oriented to cast a shadow on images A, B, C, and E, thereby accounting for the observed scatter broadening of A, C, and E, but implying that all would be vulnerable to reddening in contradiction with B being the bluest and D being the reddest of the images. The model parameters are: $p = +52^\circ$, $i = 72.5^\circ$, $V_{\text{rot}} = 250$ km s $^{-1}$, $R_c = 0.8$ kpc, (gas scale height $h = 0$ kpc), $V_{\text{off}} = -15$ km s $^{-1}$, and galaxy position at $\Delta X = 535$ mas, $\Delta Y = 290$ mas. This model has an exponential radial decline in HI column density, with scale length 1.5 kpc, from a central peak of $1.5 \times 10^{21} (T_s/100)$ cm $^{-2}$ measured perpendicular to

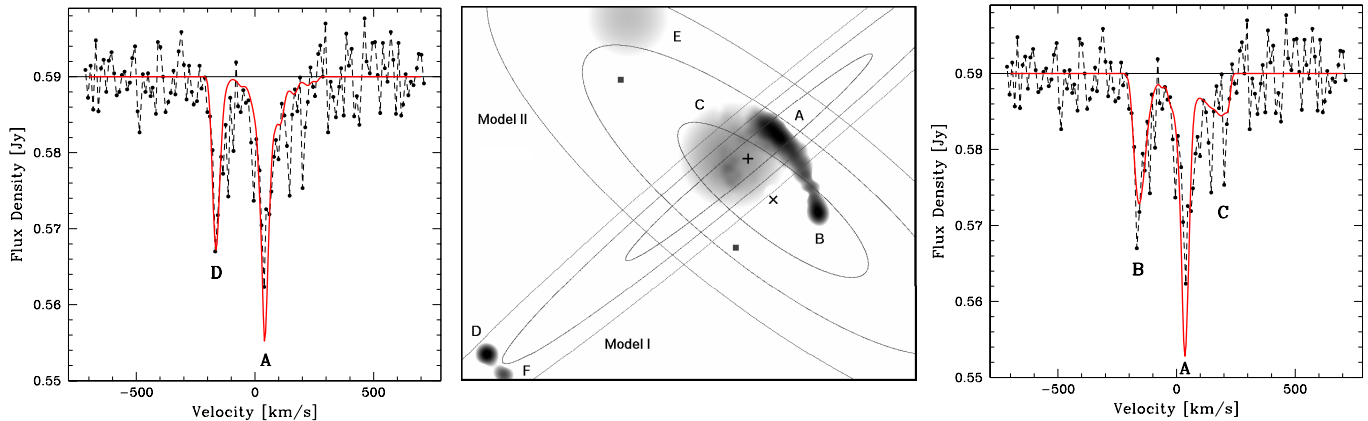


Fig. 2. Disk galaxy models for the absorption profile. Central Panel [B]: The six principal image components (A–F) of the 1.7 GHz VLBA image of W03 (grey-scale), with two sets of ellipses drawn to indicate the orientation and inclination of the intervening model disk galaxies. The galaxy centre is marked by a + and a × for Models I and II, respectively; the two filled squares indicate the mass centroids of the two mass lens model of Keeton & Winn (2003). Left Panel [A]: 21cm spectrum derived from Model I (heavy line) superimposed on the observed 21cm profile (dashed line). Right Panel [C]: 21cm spectrum derived from Model II (heavy line) superimposed on the observed 21cm profile (dashed line). In both cases, the zero of the velocity scale corresponds to 805 MHz ($z = 0.76448$, heliocentric). See text for discussion.

the disk plane. The spectrum resulting from the above orientation is shown in fig. 2[C]. Here, the two narrow features arise against images A and B, while the broad shoulder at positive velocities stems from absorption against image C and the radio arc connecting A and B.

4. Summary

The 21cm absorption line profile at $z \sim 0.7645$ towards PMN J0134–0931 has two primary components and a broad weak trough. It has a total velocity width of $\sim 500 \text{ km s}^{-1}$ and the largest HI equivalent width so far detected in a gravitational lens system. The extremely high estimated HI column density $N_{\text{HI}} = 2.6 \pm 0.3 \times 10^{21} (T_s/200\text{K})(1/f) \text{ cm}^{-2}$ suggests that the reddening of the quasar is due to dust in the $z \sim 0.7645$ lens.

None of the galaxy models that assume a single disk-like absorber have succeeded in accounting for all the observations, although the models can roughly reproduce the observed 21cm absorption profile. Specifically, Model I in Sect. 3.2 does not account for the observed scatter broadening of component E while Model II fails to reproduce the fact that D is the reddest and B, the bluest, of all images. Of course, the large 21cm velocity width of $\sim 500 \text{ km s}^{-1}$ could also arise if the absorption occurs in two separate galaxies. This is in agreement with the suggestion of Keeton & Winn (2003) that the lensing system consists of two spiral systems. Further, it is consistent with the HST image of W03 showing marginal detections of two galaxies, the northern one close to images A, C and E and the southern one near image D. For example, the northern “galaxy” in the HST image might cause the main 21cm feature and most of the broad, weak absorption, arising against images A, C, E and the radio arc, while the southern “galaxy” causes the secondary (blue-shifted) feature (and perhaps some of the broad trough), through absorption against image D. The present 21cm data do

not warrant a detailed modelling of such a two-galaxy absorption system as the number of free parameters is far larger than the number of observational constraints (especially given that the observed 21cm profile can be reproduced with a single disk galaxy model). High resolution radio interferometric observations at 805 MHz will help refine the kinematic models and shed more light on the nature of the intervening lens system.

Acknowledgements. We thank Rene Vermeulen for much help with the planning and scheduling of these WSRT service observations. We are also grateful to Josh Winn for providing the 1.7 GHz VLBA image and CC file for use in our modelling. The Westerbork Synthesis Radio Telescope is operated by the ASTRON (Netherlands Foundation for Research in Astronomy) with support from the Netherlands Foundation for Scientific Research (NWO).

References

- Baars J. W. M., Genzel R., Pauliny-Toth I. I. K., & Witzel A. 1977, A&A, 61, 99
- Binney J. J., & Merrifield M. 1998, Galactic Astronomy, Princeton University Press, Princeton, NJ
- Braun R., & Walterbos R. A. M. 1992, ApJ, 386, 120
- Briggs F. H., Wolfe A. M., Turnshek D. A., & Schaeffer J. 1985, ApJ, 293, 387
- Browne I. W. A., Patnaik A. R., Walsh D., & Wilkinson P. N. 1993, MNRAS, 263, L32
- Carilli C. L., Rupen M. P., & Yanny B. 1993, ApJ, 412, L59
- Chengalur J. N., de Bruyn A. G., & Narasimha D. 1999, A&A, 343, L79
- Gregg M. D., Lacy M., White R. L., et al. 2002, ApJ, 564, 133
- Hall P. B., Richards G. T., York D. G., et al. 2002, ApJ, 575, L51
- Kaneekar N., & Chengalur J. N. 2002, A&A, 381, L73
- Kaneekar N., & Chengalur J. N. 2003, A&A, 399, 857
- Kaneekar N., Chengalur J. N., de Bruyn A. G., & Narasimha D. 2003, MNRAS, 345, L7
- Keeton C. R., & Winn J. N. 2003, ApJ, 590, 39

- Prochaska J. X., & Wolfe A. M. 1997, ApJ, 487, 73
 Rusin D., Kochanek C. S., Norbury M. et al. 2001, ApJ, 557, 594
 Winn J. N., Lovell J. E. J., Chen H-W. et al. 2002, ApJ, 564, 143
 Winn J. N., Kochanek C. S., Keeton C. R., & Lovell J. E. J. 2003, ApJ, 590, 26
 Wolfe A. M., Turnshek D. A., Smith H. E., & Cohen R. D. 1986, ApJS, 61, 249.